Materials Today Communications 36 (2023) 106569

Contents lists available at ScienceDirect

Materials Today Communications

journal homepage: www.elsevier.com/locate/mtcomm

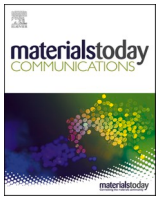

CO_2 absorption of recycled concrete aggregates in natural conditions

Andreas Leemann *, Beat Münch, Mateusz Wyrzykowski

Empa, Swiss Federal Laboratories for Materials Science and Technology, Switzerland

ARTICLE INFO

Keywords:
Concrete
Recycled concrete aggregates
CO_2 absorption
Image analysis

ABSTRACT

Cement production is linked to a substantial CO_2 emission contributing to about 5–8% of the man-made emissions. However, hardened cementitious materials can absorb CO_2 in the process called carbonation, both during the service life of the structures and during their demolition and recycling phase. As experimental data of CO_2 absorption during the recycling phase are scarce, the goal of the study is to experimentally determine the CO_2 absorption of recycled concrete aggregates (RA) from the point of crushing until reuse in recycled aggregate concrete (RC). Samples from three plants producing both RA and RC were collected and stored both in the plants and in the laboratory for several months. The change in the amount of uncarbonated cement paste of the RA with time was determined by using a novel method: image analysis of samples embedded in epoxy, ground and sprayed with phenolphthalein. This allowed to calculate the CO_2 absorption during the storage of RA. The amount of absorbed CO_2 corresponds to about 5.4–12.6% of total CO_2 emission originally stemming from the production of cement.

1. Introduction

Concrete represents a major part of today's built environment and is one of the most abundant materials on the planet [1]. Production of concrete is associated with high demand for cement – the binder in concrete. More than 600 kg of cement are produced per capita worldwide every year [2]. The production of one ton of cement clinker (the major binding phase in cement) is linked to a total CO_2 emission of 842 kg [3]. 507 kg per ton are attributable to the geogenic emission (thermal decomposition of the carbonate phases necessary to create reactive phases in cement clinker) [4], whereas the remaining part of the emissions is mainly caused by the operation of the cement kiln. As a consequence, cement production is responsible for 5–8% of the man-made CO_2 emissions [2,5–7]. One important aspect of estimating the contribution of cement to the global CO_2 balance is the fact that the hardened cement has the ability to absorb CO_2 by carbonation. As a result, part of the CO_2 originally emitted during cement production is later absorbed by concrete during the service life of structures [4–8]. The calculations for some European countries indicate absorption values of 7–19% of the geogenic CO_2 emission [8–12]. Although many assumptions have to be made for such calculations, there is a solid data base on carbonation coefficients of different concrete qualities and compositions and the effect of the environment [13–17]. The carbonation of concrete continues after demolition and crushing of concrete into recycled concrete aggregates (RA), however, the boundary conditions and hence the rate of carbonation change significantly. Due to the increase of the surface area per volume, the carbonation rate is greatly increased [8,9,12,18–22]. The grain size of the crushed concrete is not the only factor influencing CO_2 absorption of RA. A laboratory study on model materials has shown that the carbonation rate of RA is dependent on the moisture content as well [20]. Exposing RA to drying and wetting cycles in the laboratory accelerates carbonation at natural CO_2 level [19]. In addition to the beneficial effect of CO_2 absorption by RA on the environment, the use of carbonated RA has been shown to improve the quality of recycling concrete and pavements [23–29]. There are several studies assessing the CO_2 uptake of concrete during the recycling and demolition phase. For the Northern European countries it has been estimated that 6–33% of the original geogenic CO_2 is absorbed during the recycling phase in addition to the absorption during service life [9]. An estimation for the situation in Switzerland considering four different scenarios resulted in values of 6–15% (respect to the original geogenic emissions of cement) with the assumption that 70% of the demolished concrete is recycled and reused as RA [12]. Based on the conditions present in South Korea, it was assessed that an amount of 20–23% of the geogenic CO_2 emission is absorbed [22]. However, due to the scarcity of experimental data, such studies rely heavily on assumptions in regard to CO_2 absorption during the demolition and recycling phase. This results in a high degree of uncertainty for such results. Experimental data on RA

* Corresponding author.
E-mail address: andreas.leemann@empa.ch (A. Leemann).

https://doi.org/10.1016/j.mtcomm.2023.106569
Received 24 April 2023; Received in revised form 2 June 2023; Accepted 28 June 2023
Available online 29 June 2023

exposed to natural conditions in recycling plants before their reuse are needed in order to improve the data base.

The goal of this study is to determine the CO_2 absorption of RA during storage in natural conditions. The change in the degree of carbonation of three different RA was analyzed during an exposure time of several months. The major part of the RA were stored in concrete plants and subsamples were stored sheltered and unsheltered at the laboratory facility. Grain size distribution, water absorption and bulk density of the RA were determined. The amount of uncarbonated cement paste in the RA particles was determined with image analysis of embedded and ground particles sprayed with phenolphthalein. We developed a novel approach for image segmentation using 3-dimensional color space (HSV) that allowed to take advantage of the distinct colors originating from green resin and pink coloring of uncarbonated paste caused by phenolphthalein. Based on the change in the degree of carbonation of the RA during storage, the CO_2 absorption was calculated for different RA types. These results enable assessing contribution of CO_2 absorption in recycling phase to the overall CO_2 emissions balance of cement.

2. Materials and methods

2.1. Materials

A survey in eight concrete plants showed that five plants store RA unsheltered and three sheltered. The duration between crushing and use of the RA for concrete production ranges from 0.5 to 12 months, with an average of three months. Based on this situation, the duration of exposure for the RA studied in the project was chosen as described in the following.

Three industrially produced RA (RA-1, RA-2, RA-3) from established producers of RA and RC (plant-1, plant-2, plant-3) were studied. In plant-1 decommissioned railway sleepers were available for crushing. The concrete available for crushing in plant-2 and plant-3 mainly originated from the demolished buildings. After crushing and sieving, the RA were stored at the respective plants. In plant-1, the pile of RA-1 was more than 30 m wide and about 5 m high. In plant-2, the pile of RA-2 was about 14 m wide and about 2.5 m high. In both cases, the piles were not sheltered and accordingly exposed to the weather. Annual rainfall at the location of the plants and in the courtyard of the laboratory facility of Empa is about 1000 mm. RA-3 (0–16 mm) in plant-3 was stored sheltered in plastic containers with a width of 10 × 14 m^2 and a height of 7.5 m. However, it has to be pointed out that the demolished concrete was stored unsheltered for a few months and the crushing was performed unsheltered as well. Consequently, the concrete was exposed to the weather before being moved to sheltered conditions.

Batches of RA-1 (~ 250 kg) and RA-2 (~ 75 kg) were delivered in airtight bags to Empa a few days after crushing and sieving. The RA were stored at Empa in layers with a thickness of ~ 25 cm (RA-1) and ~ 10 cm (RA-2), both outside in sheltered and unsheltered exposure. A layer thickness of only ~ 10 cm was chosen in the case of RA-2 due to the relatively small sample size. The first analysis of degree of carbonation was performed right after receiving the RA from the plants (Fig. 1). The samples stored at Empa were analyzed additionally after 1.5 and 6 months of exposure. The entire layer thickness of the beds of RA was sampled. Samples from the piles in the plant were analyzed after 6 months (RA-1) and after 8 months (RA-2). This included samples taken close to the surface of the pile (depth of 0–25 cm) and from the inner part of the piles (depth 1.5–2.5 m). RA was removed by a digger to reach the inner part of the pile.

No samples were taken in plant-3 right after crushing. Two months after crushing, samples of RA-3 were taken from a depth 0–25 cm and from ~1.0–1.2 m and delivered to Empa in airtight bags. Images of RA-1 and RA-3 are shown in Fig. 2.

2.2. Methods

2.2.1. General

A sample of about 40 kg of each RA was taken, homogenized and subsamples were used for the different tests described in the following (Fig. 3).

The moisture content of the RA as delivered after exposure was determined by drying approximately 3 kg in an oven at 110 °C for 24 h. The 3 kg were taken from a homogenized sample of about 20 kg. The grain size distribution of the RA was determined with sieving according to EN 933–1 [30]. Bulk density and water adsorption were determined on the grain size classes 0–4, 4–8, 8–16 and 16–22 mm according to EN 1097–6 [31].

The different grain size classes obtained by sieving were used for the analysis of the degree of carbonation. The duration of exposure to air was kept as short as possible to reduce the carbonation in the entire process from taking the samples to embedding them in epoxy.

2.2.2. Sample preparation for determining degree of carbonation

The typical aggregates used in the Swiss Midland from which the RA in this study originate contain a substantial amount of $CaCO_3$

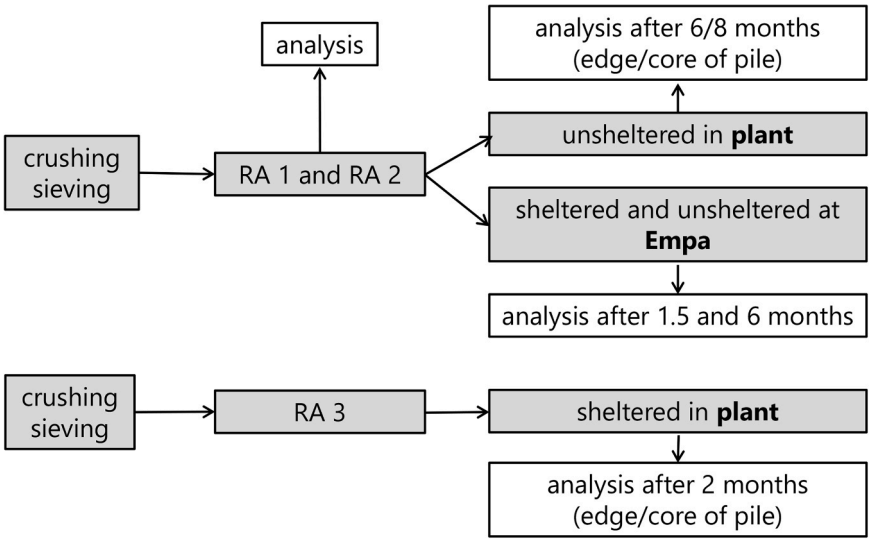

Fig. 1. Type of storage and time of analysis of the different RA.

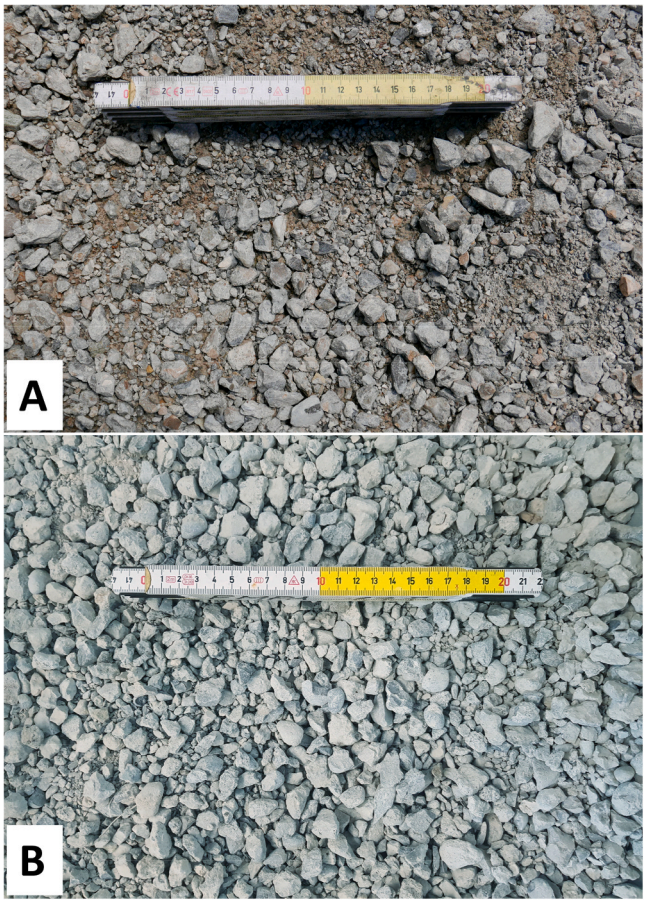

Fig. 2. Recycled aggregate RA-1 after an exposure of 1.5 months at Empa (A) and recycled aggregate RA-3 as delivered to Empa (B).

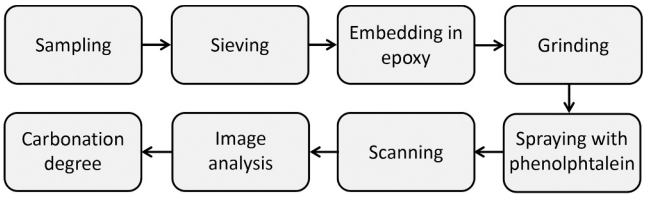

Fig. 3. Flow chart showing the sequence of sample preparation and analysis (see also Fig. 5 for the detailed steps of image analysis).

(approximately 40 mass-%). This excludes thermogravimetric analysis (TGA) as a method to determine the amount of $CaCO_3$ formed by the carbonation of portlandite, calcium-silicate-hydrate (C-S-H) and ettringite, as the TGA signal from these products would overlap with that of the aggregates. At the same time, TGA allows only to accurately determine the amount of portlandite in uncarbonated cement paste but not the amount of C-S-H and ettringite. Therefore, an alternative approach was chosen and the amount of uncarbonated cement paste in the RA-particles was determined with image analysis on samples sprayed with phenolphthalein.

RA-particles from the grain size classes 0–4, 4–8, 8–16 and 16–22 mm were embedded in epoxy resin containing a green dye. 15 g of the sand (0–4 mm) was put into a plastic container with an inner base area of 8.5 × 10.3 cm^2 resulting in a layer with particles lying on top of each other. The coarser fractions were placed in plastic containers with an inner base area of 10.8 × 14.4 cm^2. The particles were carefully placed next to each other creating a single particle layer. After placing the particles, the containers were flooded with epoxy. They were placed in a water bath during the hardening of the epoxy to cool them and prevent the formation of air bubbles due to heat generation. After hardening, the bottom of the container and part of the epoxy-impregnated aggregates were removed by grinding under water. The layer thickness of the impregnated aggregates removed by grinding was 1 mm in the case of the sand and one third of D_{max} of the coarser grain size class (e.g. ~ 5.3 mm in the case of 8–16 mm). The layer to be removed by grinding was marked on the outside of the containers before the process to establish reference points. After wet grinding, the samples were put in an oven at 40 °C for 30 min to remove the water from the preceding grinding. In the next step, the samples were carefully sprayed with small amount of phenolphthalein that was adsorbed by capillary suction of the dry RA. The sprayed samples were put into an air tight zip lock bag for 24 h. In a next step the ground surface was cleaned using a brush and isopropanol. The ground surface was sprayed with isopropanol to enhance color saturation and contrast and was scanned with a flatbed scanner. While a resolution of 2400 dpi was chosen for the sand fraction, 1200 dpi were used for the coarser particles.

2.3. Image analysis

Initially, a segmentation of the scan into three distinct regions is achieved: (1) epoxy resin, (2) material with original color exhibited by concrete (carbonated cement paste and primary aggregates), and (3) pink colored material (uncarbonated cement paste). The high saturations of the green epoxy resin and of the magenta colored uncarbonated cement paste are the key characteristics for an unambiguous classification. The HSV (h: hue, s: saturation, v- value, [32]) color space is particularly convenient for proper finding of the distinct boundaries of the respective color gamut. The top image of Fig. 4 illustrates the layer of the 3D HSV color space at highest brightness (i.e. at highest v). The bottom image illustrates the typical color distribution of a concrete mix (here Jura 0/4 mm). The segmentation is effected in two steps: the first step is the division of concrete and epoxy resin representing the background; the second step is the division of the concrete class into subclasses of carbonated (including the natural aggregate particles in the RA) and uncarbonated. The magenta color gamut effectuated by dyeing with phenolphthalein can be isolated by a single h,s-color sector (including all brightness values v) into the HSV color space (see lower right sector in both illustrations of Fig. 4). The zones delimiting the epoxy resin (colored from bright green to yellow) were determined by three color sectors at different ranges of brightness (see upper sectors in the illustrations of Fig. 4). Refined elaboration using three sectors was particularly necessary due to the fraction 0/4 mm containing finest dust particles mixed with epoxy resin which are severely complicating a straightforward distinction of epoxy resin and concrete granules. The unique choice of the color sectors was selected by visual assessment. Their position and size was uniformly defined such that optimal segmentation was achieved over all evaluated scans. Uniform definition of the sectors allows direct quantitative comparison between any measurements of any fractions. The boundaries of the chosen color sectors are listed below (the values h,s,v are normalized to the interval [0.1], respectively).

HSV sectors for delimiting the aggregates from the epoxy resin in the background:

1. $(h_{min}…h_{max}, s_{min}…s_{max}, v_{min}…v_{max}) = (0.22…0.4, 0.65…1, 0.4…1)$
2. $(h_{min}…h_{max}, s_{min}…s_{max}, v_{min}…v_{max}) = (0.16…0.4, 0.85…1, 0.5…1)$
3. $(h_{min}…h_{max}, s_{min}…s_{max}, v_{min}…v_{max}) = (0.16…0.4, 0.50…1, 0.9…1)$

HSV sector for delimiting the uncarbonated regions from the other regions:

1. $(h_{min}…h_{max}, s_{min}…s_{max}, v_{min}…v_{max}) = (0.7…1, 0.1…1, 0.2…1)$

The images of the concrete granule scans are afflicted by a certain

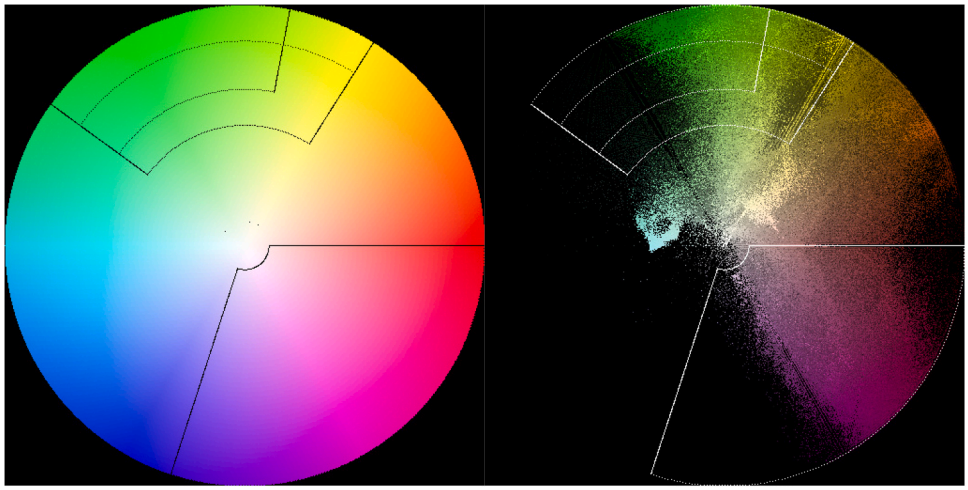

Fig. 4. h-s-plane of the HSV color space at maximal brightness v (top), h-s-distribution from the pixel values of a typical concrete granulate scan (bottom).

noise. To remove the noise, the binary masks being identified by the above procedure subsequently undergo a morphological post processing by eliminating all regions smaller than a certain threshold size (see Table 1).

The implemented processing steps are displayed in Fig. 5. From each color scan (A), the image values are converted from Adobe RGB (B) to the HSV color space (C). Subsequently, the values are split into two color sectors, the first one containing granules (D) and the second one containing epoxy resin (E). Subsequently, the image values belonging to the granules class are further divided into "uncarbonated" (F) and "carbonated" (G) color sectors. Finally, the images belonging to the respective color spaces are being reconstructed (H: epoxy resin, I: uncarbonated, J: carbonated) (Fig. 6).

2.4. Volume of carbonated paste and estimation of error

The change in the amount of uncarbonated paste of the RA-particles was determined for each grain size class. The reference for RA-1 and RA-2 were the values determined right after delivery. As no samples were taken from RA-3 immediately after crushing, an alternative approach was used in this case. As the degree of carbonation decreases considerably with increasing particle size, the amount of uncarbonated cement paste in the largest grain size class (16/32 mm) was chosen as reference. This may cause a minor underestimation of the degree of carbonation of RA-3.

The measurements were carried out at different ages on different types of RA using single specimens only (see values in Table 4). Yet, in order to assess the error of the method, a larger number of specimens was studied initially. To this end, six specimens per each of the three grain size classes of RA-1 (0–4, 4–8 and 8/16 mm) and four specimens of RA-2 (grain size class 4/8 mm) were measured.

The values for volume percentage of uncarbonated paste in the RA-particles were (average ± standard deviation) 12.5 ± 2.77% (RA-1, 0–4 mm), 30.5 ± 2.47% (RA-1, 4–8 mm), 28.5 ± 3.56% (RA-1, 8–16 mm) and 14.0 ± 1.46% (RA-2, 4–8 mm). As no trend in the standard deviation between the different fractions/types of RA was apparent, we assumed that the pooled standard deviation from these data (22 specimens in total), equal to 2.78 vol%, corresponds to a representative error. Then, considering that the determined values of carbonated paste volume and CO_2 absorption are based on single specimens, we estimated the propagation of the error in the determination of the uncarbonated volume-% using parametric bootstrapping [33]. In each of the bootstrapping steps (with a total of 10000 steps), samples of six specimens were simulated assuming a normal distribution with standard deviation equal to the pooled value of 2.78 vol%. This procedure yielded the 95% confidence intervals presented together with the experimental results (in Figs. 10–12 and Table 5).

Table 1
Minimum object size in number of pixels for all examined fractions.

fraction [mm]	minimum object size [# pixels]
0/4	15
4/8	60
8/16	250
16/32	1000

2.5. Calculation of CO_2 absorption

An assumption for the amount of cement clinker in the cement paste of RA has to be made to enable a calculation the CO_2 absorption due to carbonation. In the case of RA-1, the type of source concrete was known. Railway sleepers with a strength class of C40/50, C50/60 und C60/75 were processed to RA. An average Portland cement content of 380 kg/m^3 of concrete and a water-to-cement-ratio (w/c) of 0.42 were assumed. The clinker content of the PC was assumed as 95 mass-% [34]. Portland cement with such percentage was the dominating cement type > 30 years before today in Switzerland.

The source of RA-2 and RA-3 was concrete used for housing. Nowadays about 95% of the concrete produced in Switzerland are type A (cement content ≥ 280 kg/m^3, w/c ≤ 0.65), type B (cement content ≥ 280 kg/m^3, w/c ≤ 0.60) and type C (cement content ≥ 300 kg/m^3, m w/c ≤ 0.50) according to SN EN 206–1:2013 [35]. The share of type A and C are about equal and type B amounts to only a third of each of the two other types [12]. Based on this, a Portland cement content of 300 kg/m^3 of concrete and a w/c of 0.55 was assumed for the composition of RA-2 and RA-3.

The starting point to calculate CO_2 absorption of the RA is the volume of cement paste V_{cp} in the source concrete.

A typical density for PC is $\rho = 3.14$ g/cm^3. Air void content V_{AV} is assumed to be 2.0 vol%. This results in a cement paste content of 0.301 m^3/m^3 for RA-1 and 0.281 m^3/m^3 for RA-2 and RA-3, using the following equation:

$$V_{cp} = c/\rho + w + V_{AV} \quad (1)$$

with c = cement content, w = water content and V_{AV} = air void content.

The amount of CaO in the cement clinker is calculated according to the data given in [34]:

$$\mathrm{CaO} = c \cdot 0{\cdot}95 \cdot 0{\cdot}65 \quad (2)$$

The CaO originally present in the clinker and then in the cement

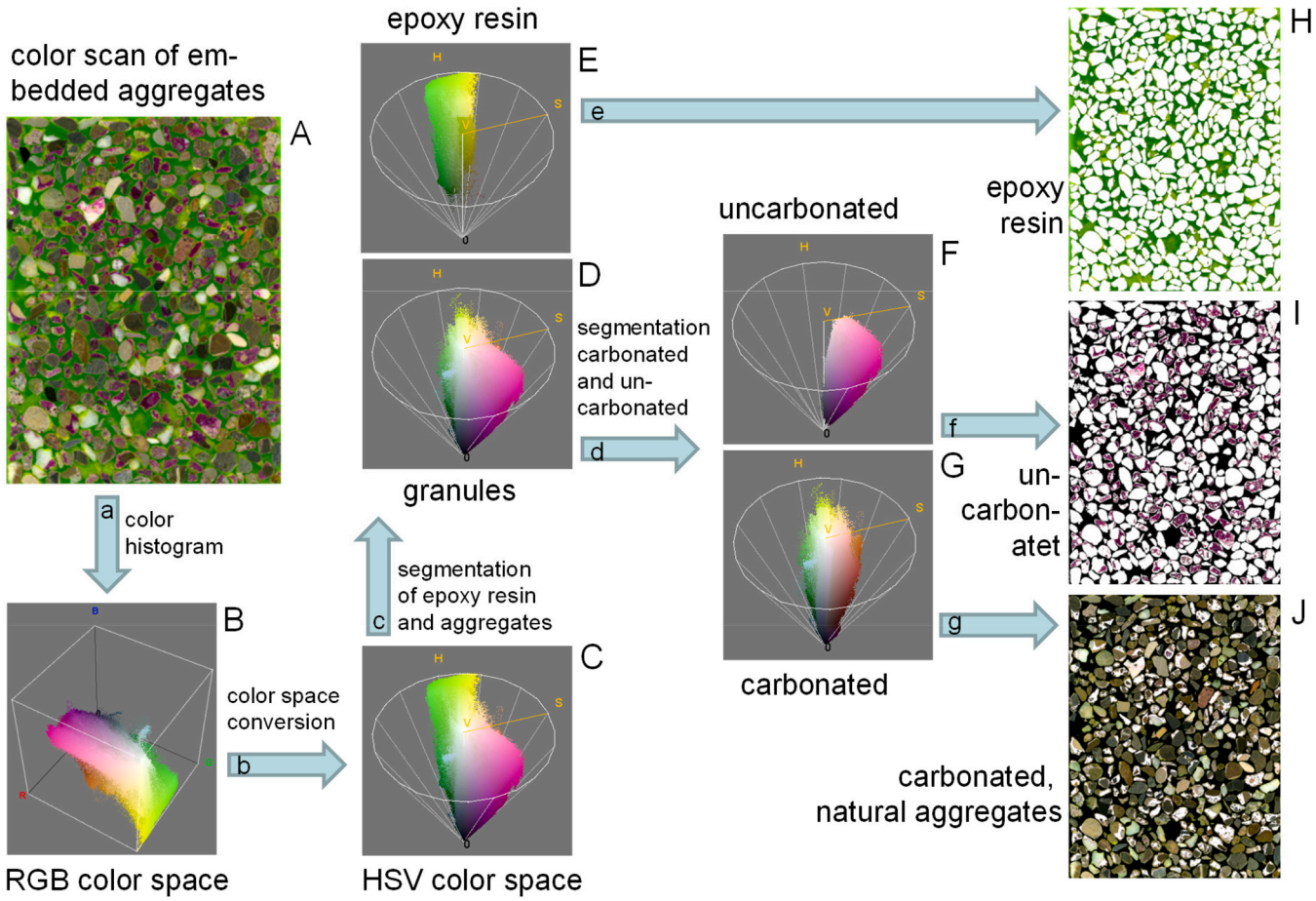

Fig. 5. Segmentation of concrete granules for the distinction of (H) epoxy resin, (I) uncarbonated as well as (J) carbonated cement paste including natural aggregates.

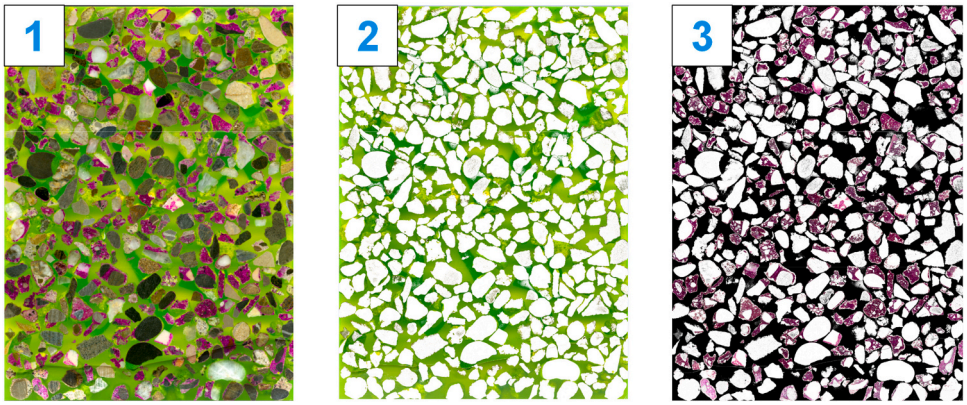

Fig. 6. Image analysis steps for the segmentation of an example fraction 4/8 mm: 1 = original scan, 2 = segmentation of aggregates, 3 = segmentation of uncarbonated parts of aggregates (see "A", "H", "I", respectively, in Fig. 5).

hydrates is only partially converted to $CaCO_3$ upon carbonation in atmospheric conditions [36]. In [8] a value of 75% was used. Experimentally determined values differ. A value of 55% was determined in [20] for a mortar produced with CEM I. There seems to be a certain dependence on the water-to-cement-ratio (w/c), as indicated by values of 52% in mortar produced with PC and a w/c of 0.48 opposed to a value of 65% in a mortar produced with PC and a w/c of 0.65 [37]. On the other hand, there may be already partial carbonation in the cement paste that still turns to magenta when sprayed with phenolphthalein [38,39]. In this study, it was assumed that 60% of the CaO present in the clinker reacts with CO_2 to form $CaCO_3$ in the carbonated cement paste. Furthermore, values of 507 and 842 kg were used for the geogenic [4] and for the total CO_2 emission [3] during production per ton of clinker to enable comparing the absorbed CO_2 to the original emissions of concrete.

An example calculation for CO_2 absorption due to carbonation is given using RA-2.

In this example the change in the amount of uncarbonated cement paste in the total volume of RA-2 from time t_0 to t_1 changes from 20.0 to 12.5 area-% of the entire aggregate particles. As area-% equates volume-

% according to the Delesse principle [40], this corresponds to a difference of 7.5 vol%. The volume of cement paste in RA-2 equals 0.278 m^3/m^3. Accordingly, the volume of cement paste carbonated from t_0 to t_1 is:

$$V_{cp,carb} = 7{\cdot}5/0{\cdot}278 = 27{\cdot}0 \text{ vol\%} \quad (3)$$

The amount of carbonated CaO in this volume per m^3 of concrete, assuming that 60% of CaO carbonates, is calculated as:

$$CaO_{carb} = 300 \text{ kg/m}^3 \cdot 0{\cdot}95 \cdot 0{\cdot}65 \cdot 0{\cdot}60 \cdot 0{\cdot}27 = 30{\cdot}0 \text{ kg/m}^3 \text{ RA} \quad (4)$$

This corresponds to an amount of absorbed CO_2 of 23.6 kg/m^3 of RA (molar mass CO_2 = 44 g and CaO = 56 g). If the RA density of 2380 kg/m^3 is assumed, the amount of absorbed CO_2 is 9.9 kg/t of RA. This further corresponds to 16.4% absorbed CO_2 relative to the geogenic emission of the original concrete (507 kg CO_2 per ton of clinker).

3. Results

3.1. Grain size distribution

RA-1 and RA-3 correspond to the grain size class 0–16 mm with a minor part of particles > 16 mm and RA-2 corresponds to the grain size class of 0–22 mm (Fig. 7). RA-1 contains the highest amount of sand (0–4 mm) followed by RA-3 and RA-2.

3.2. Bulk density and water adsorption WA_{24}

There is a general trend of decreasing bulk density and increasing water adsorption WA_{24} with decreasing grain size in all three RA (Table 2). This is a result of a slightly increasing cement paste content with decreasing grain size.

If the grain size distribution is taken into account, the average of WA_{24} are 4.30, 4.38 und 4.74% for RA-1, RA-2 and RA-3.

3.3. Moisture content at delivery

The moisture content of the RA at the time of delivery after exposure in the plants is shown in Table 3. In all cases the moisture content at the edge of the pile is lower than in the interior, where the values are well above the water adsorption WA_{24}. At the edge of the pile the moisture content in RA-1 is slightly below and in RA-2 slightly above WA_{24}. Only in the case of RA-3 stored in sheltered conditions the moisture content is about half of WA_{24}.

3.4. Degree of carbonation

The amount of uncarbonated cement paste in the RA-particles decreases only in the sand fraction in case of RA-1 (Table 4). There is no carbonation at all in the grain size classes 4–8 and 8–16 mm (Fig. 8). The variations in the amount of uncarbonated paste at a grain size > 4 mm are caused primarily by differences in the ratio between uncarbonated paste and natural aggregates included in the RA-particles. There is no significant difference in the degree of carbonation of the RA-1 sand between sheltered and unsheltered exposure of the samples stored at the laboratory. Moreover, there is no difference in the degree of carbonation between the samples taken from the edge and the interior of the pile in the plant. Generally, the samples stored at the plant have a slightly higher degree of carbonation than the samples stored at Empa.

RA-2 shows a rapid CO_2 absorption in the sand fraction, leading the nearly complete carbonation after 1.5 months (Table 4). RA-2 4–8 mm and 8–16 mm show a decreasing amount of uncarbonated paste as well. However, the decrease is less pronounced than in the sand. No carbonation is observed in the grain size class 16–22 mm. The samples from the edge and the interior of the pile show no difference in the degree of carbonation. However, the amount of uncarbonated paste in the RA-particles is higher compared to the samples stored at Empa.

The amount of uncarbonated cement paste in the RA-particles of RA-3 decreases with grain size (Table 4). Here, the RA-particles at the edge of the pile show a higher degree of carbonation. An example of the grain size class 4/8 mm of RA-3 is given in Fig. 9.

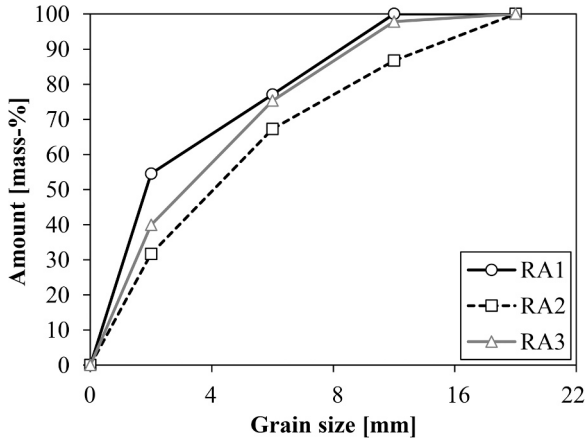

Fig. 7. Grain size distribution of the three RA.

Table 2
Apparent density (AD), bulk density (BD) oven dried and water adsorption after 24 h (WA_{24}) according EN 1097–6 for the different grain size classes and the aggregate 0-d_{max} taking into account the grain size distribution presented in Fig. 7.

		0/ 4 mm	4/ 8 mm	8/ 16 mm	> 16 mm	0- d_{max}
RA-1	*AD* [kg/m³]	2.69	2.68	2.67	-	2.68
	BD [kg/m³]	2.37	2.42	2.44	-	2.40
	WA_{24} [mass-%]	4.92	3.99	3.49	-	4.30
RA-2	*AD* [kg/m³]	2.67	2.64	2.66	2.64	2.65
	BD [kg/m³]	2.35	2.38	2.44	2.40	2.38
	WA_{24} [mass-%]	5.12	4.19	3.47	3.85	4.38
RA-3	*AD* [kg/m³]	2.71	2.70	2.69	-	2.70
	BD [kg/m³]	2.33	2.42	2.47	-	2.40
	WA_{24} [mass-%]	6.00	4.30	3.31	-	4.74

Table 3
Moisture content of the RA after exposure at the time of delivery. Water adsorption (Table 2) is shown for comparison.

	RA-1	RA-2	RA-3
	[mass-%]	[mass-%]	[mass-%]
edge	3.8	5.9	2.6
interior	6.1	10.4	7.8
WA_{24}	4.3	4.4	4.7

4. Discussion

4.1. Carbonation

The amount of uncarbonated cement paste in the RA-particles of the sand fraction at time t_0 is lower than of the grain size classes ≥ 4 mm with average values of 22.8 (0–4 mm) and 28.9% (> 4 mm) for RA-1 and 12.9 (0–4 mm) and 18.4% (> 4 mm) for RA-2. The amount of uncarbonated cement paste at the time of crushing can be expected to be the same in all grain size classes. Obviously, some carbonation took place between crushing and analysis in spite of the fact that the samples were delivered from the plants to Empa within a few days. Additionally, a minor carbonation in the laboratory cannot be excluded during the

Table 4
Amount of uncarbonated cement paste in total volume of RA-1 and RA-2 stored at the Empa and in the plant. A representative error (standard deviation) is estimated as ± 2.78 vol% (see Section 2.4 for details). In the grain size classes 4/8 and 8/16 mm of RA-1 no carbonation was observed. The grain size class 16/32 mm of RA-3 was used as reference for the smaller grain size classes.

	Time	[month]	t_0	$t_{1.5\,m}$	$t_{6/8\,m}$ [a]	$\Delta\ t_0$-t_{final}
RA-1 uncarbonated paste [volume-%]	Empa sheltered	0–4 mm	22.8	14.9	12.5	10.3
	Empa unsheltered	0–4 mm		15.3	13.7	9.1
	Empa sheltered	4–8 mm	30.7	no carb.	no carb.	0.0
	Empa unsheltered	4–8 mm		no carb.	no carb.	0.0
	Empa sheltered	8–16 mm	27.1	no carb.	no carb.	0.0
	Empa unsheltered	8–16 mm		no carb.	no carb.	0.0
	Plant, edge of pile	0–4 mm	22.8	-	10.9	11.9
	Plant, interior of pile	0–4 mm		-	11.0	11.8
	Plant, edge of pile	4–8 mm	30.7	no carb.	no carb.	0.0
	Plant, interior of pile	4–8 mm		no carb.	no carb.	0.0
	Plant, edge of pile	8–16 mm	27.1	no carb.	no carb.	0.0
	Plant, interior of pile	8–16 mm		no carb.	no carb.	0.0
RA-2 uncarbonated paste [volume-%]	Empa sheltered	0–4 mm	12.9	1.7	0.9	12.0
	Empa unsheltered	0–4 mm		1.8	0.0	12.9
	Empa sheltered	4–8 mm	17.6	13.1	11.3	6.3
	Empa unsheltered	4–8 mm		14.0	11.7	6.9
	Empa sheltered	8–16 mm	19.1	12.9	10.7	8.4
	Empa unsheltered	8–16 mm		14.8	12.5	6.6
	Empa sheltered	16–22 mm	20.8	20.5	20.9	-0.4
	Empa unsheltered	16–22 mm		20.0	20.5	0.3
	Plant, edge of pile	0–4 mm	12.9	-	4.7	8.2
	Plant, interior	0–4 mm		-	4.2	8.7
	Plant, edge of pile	4–8 mm	17.6	-	16.1	1.5
	Plant, interior of pile	4–8 mm		-	15.7	1.9
	Plant, edge of pile	8–16 mm	19.1	-	14.3	4.8
	Plant, interior of pile	8–16 mm		-	14.7	4.4
	Plant, edge of pile	16–22 mm	20.8		21.2	-0.4
	Plant, interior of pile	16–22 mm			20.3	0.5
RA-3 uncarbonated paste [volume-%]	Plant, edge of pile	0–4 mm	19.9	-	6.9	12.9
	Plant, interior of pile	0–4 mm		-	7.6	12.3
	Plant, edge of pile	4–8 mm		-	11.4	8.5
	Plant, interior of pile	4–8 mm		-	14.2	5.7
	Plant, edge of pile	8–16 mm		-	14.2	5.6
	Plant, interior of pile	8–16 mm		-	18.1	1.8
	Plant, edge of pile	16–32 mm		-	-	-
	Plant, interior of pile	16–32 mm		-	-	-

[a] RA-1 was exposed for 6 m, RA-2 was exposed at for 6 m at Empa and for 8 m in the plant, RA-3 was exposed for 2 m.

homogenization of the samples and sieving prior to embedding the RA-particles in epoxy in spite of minimizing the exposure duration to air. This leads to a certain underestimation of carbonation after crushing. However, this effect is not considered and only the carbonation after time t_0 is used for the calculation in case of RA-1 and RA-2. As there is no analysis at time t_0 for RA-3, the amount of uncarbonated cement paste in the RA-particles of the grain size class 16–32 mm is used as the reference at time t_0.

The moisture content of the RA as delivered after exposure in the plant is high with some of the values exceeding WA_{24}. As such, the RA particles contain adsorbed water on their surfaces and in the inter-granular spaces. The moisture content at the edge in the case of the RA stored outdoors can be expected to vary depending on the duration and intensity of the last rainfall. Moist RA in a pile dry only slowly as shown by the values for RA-3. Even after a sheltered storage of 2 month, the moisture content was still double of WA_{24} at a depth of ~ 1 m and about half at the edge of the pile indicating very slow drying. RA-3 was the only sample that shows a higher degree of carbonation at the edge of the pile compared to the interior. This can be attributed to the low moisture content at the edge. With about 55% of WA_{24} it is the sample with the lowest value of all samples (Table 3). The obviously slow drying of moist RA in sheltered conditions limits the benefit of this type of storage compared to storage in unsheltered conditions in order to increase CO_2 absorption. Anyway, in spite of the high moisture content in the case of

Fig. 8. Grain size class 4–8 mm of RA-1 from the edge of the pile after an unsheltered storage of 6 month as scanned for analysis (enlarged section: 2.1 × 3.5 cm^2). Uncarbonated paste in magenta.

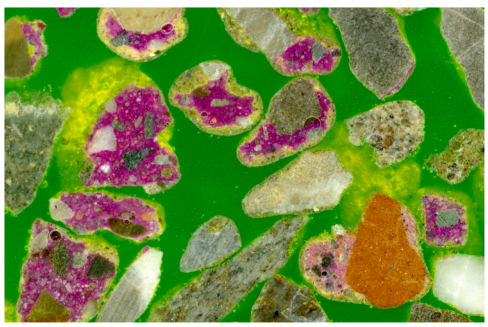

Fig. 9. Grain size class 4–8 mm of RA-3 from the interior of the pile after a sheltered storage of 2 month as scanned for analysis (enlarged section: 2.0 × 3.1 cm^2). Uncarbonated paste in magenta.

all other samples, RA still carbonate. Particles ≥ 4 mm of RA-1 produced from high quality concrete do not carbonate at all based on the pH indicator, both stored unsheltered and sheltered, while particles ≥ 4 mm of RA-2 and RA-3 still carbonate. This behavior is comparable to concrete components. Concrete specimens stored at different relative humidity in accelerated conditions (4% CO_2) show a considerable decrease in the carbonation coefficient going from 57% RH to 80% RH. However, the decrease is strongly dependent on concrete quality [15]. While carbonation at 80% RH essentially stops in case of concrete produced with a w/c of 0.40 due to capillary condensation in its pores, lower quality concrete produced with a w/c of 0.65 still carbonates, although at a slower rate. In contrast to this, fines or powders react differently as a function of RH than coarse particles. Portlandite and calcium-silicate-hydrate in powder form carbonate considerably faster at 91% RH compared to 57% [41]. Such an effect seems to be observed in RA-1, where the sand fraction carbonates in spite of the lack of carbonation observed in the grain size ≥ 4 mm. Carbonation of the RA slows down with time, as it can be expected from a process that follows a square root of time law, at least in sheltered conditions [13,14,22]. RA-1 and RA-2 show a lower rate of carbonation between 1.5 and 6/8 months compared to 0–1.5 months. About 80% of the carbonated cement paste at the end of storage was already carbonated after 1.5 months.

The small differences in the degree of carbonation between the edge and the interior of the piles in the plants indicate that CO_2 is available at least to a depth of 1.5–2.5 m (RA-1 and RA-2) in comparable amounts to cause a comparable degree of carbonation. The amount of voids in a pile of crushed aggregates 0–32 mm typically ranges from 27 to 33 vol% [42]. These voids most likely provide a connected network enabling a penetration of air even at the high moisture contents. It can be expected that the changes in the air pressure caused by wind and temperature gradients generate an air flow in the pile that considerably accelerates CO_2 transport to the aggregates.

The degree of carbonation of RA-1 stored at Empa and in the plant show a good agreement. However, RA-2 carbonated less in the plant compared to Empa. This is likely caused by the relatively low amount of RA-2 delivered to Empa. The layer of RA exposed at Empa was only ~ 10 cm in thickness. The layer sampled at the edge of the pile in the plant represents the outermost ~ 25 cm of the pile. This effect can be explained by a gradient in the degree of carbonation within the few outermost centimeters of a pile. If the particles in the outermost 2–4 cm display an increased degree of carbonation, this effect is visible in a layer thickness of ~ 10 cm, while it is obscured in a layer thickness of ~ 25 cm. However, such a layer of increased carbonation degree is of minor importance for the CO_2 absorption of the entire pile.

4.2. CO_2 absorption during storage

Based on the changes in the amount of uncarbonated cement paste in the RA-particles, their CO_2 absorption can be calculated using the approach detailed in paragraph 2.5 with the error assessment (bootstrap 95% confidence intervals) as outlined in paragraph 2.4. The values for the three RA are shown in Figs. 10–12.

Based on the assumed clinker content per volume of cement paste and accounting for the percentage of different size classes in a RA type (Fig. 7), the absorbed CO_2 can be related to the geogenic and the total CO_2 emissions during cement production. These values are presented for the plant-stored RA in Table 5.

These numbers apply to RA. However, not all concrete is recycled. It is assumed that demolished concrete not used for RA production is buried in disposal sites and therefore does not carbonate significantly. In [12] CO_2 absorption for three levels of recycling rates was calculated: 40%, 70% and 100%. The values of 5.4–12.6% absorbed CO_2 in relation to total CO_2 emission at a recycling rate of 100% decrease to 3.8–8.8% at a recycling rate of 70% and to 2.5–5.0% at a recycling rate of 40%. These values are included in (Fig. 13) (see also [12]). The values are in the same range as CO_2 absorption calculated based on data from Kikuchi [19] (scenario a), hypothetical CO_2 absorption of RA during a two week storage (scenario b) and observation of the degree of carbonation of RA evaluated on thin sections of two randomly chosen RA (scenario c).

The percentage of absorbed CO_2 in relation to the geogenic emission during recycling in North of Europe is assessed to be 15% (Sweden), 17% (Norway), 33% (Denmark) and 6% (Iceland) [9]. The recycling rate in Switzerland is estimated to be between 65% and 90%, depending on the region. Assuming a recycling rate of 80%, between 7.1% and 16.7% of the geogenic emission is absorbed based on the values presented in Table 5. This is in the same range as the numbers for Sweden (15%), Norway (17) and Iceland (6%) [9].

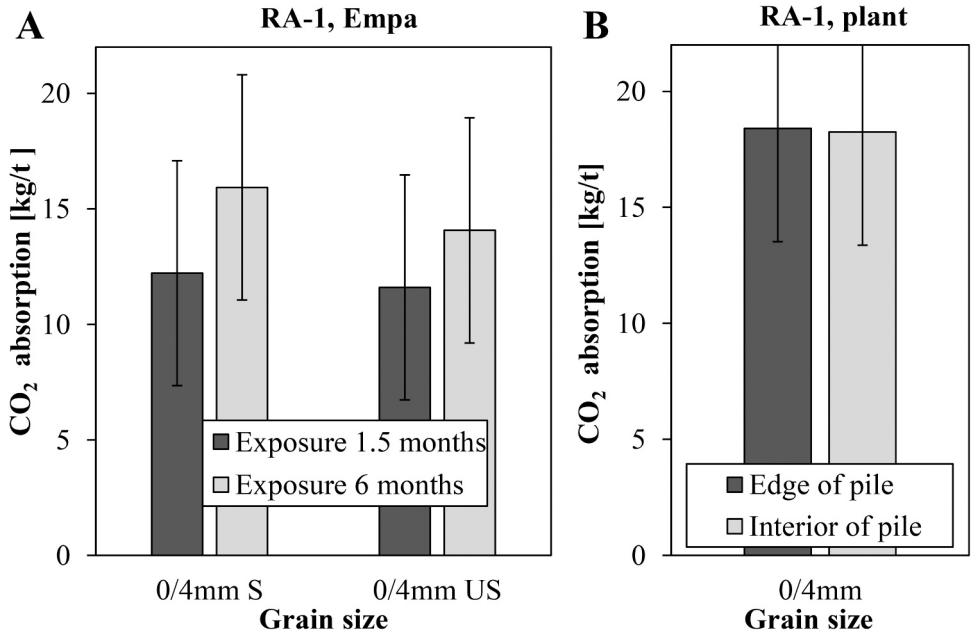

Fig. 10. CO_2 absorption in kg per ton of RA-1 (grain size class 0–4 mms) at Empa after 1.5 and 6 months in sheltered (S) and unsheltered (US) exposure and in the plant after 6 months. Grain size classes 4–8 mm and 8–16 mm are not shown as no carbonation was visible.

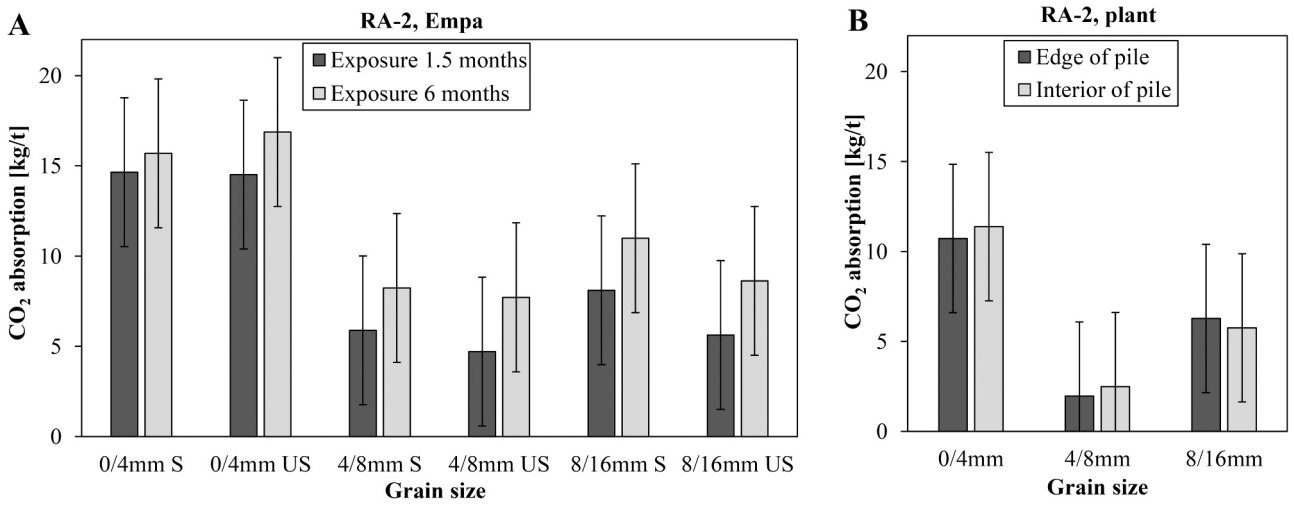

Fig. 11. CO_2 absorption in kg per ton of RA-2 at Empa after 1.5 and 6 months in sheltered (S) and unsheltered (US) exposure and in the plant after 8 months for the different grain size classes.

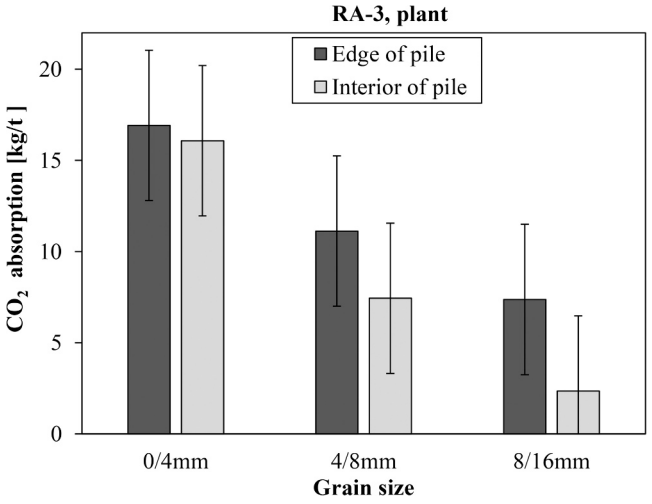

Fig. 12. CO_2 absorption in kg per ton of RA-3 of the different grain size classes after 2 months of exposure in the plant in sheltered conditions.

4.3. CO_2 absorption before time t_0

Image analysis provides the amount of uncarbonated cement paste in the RA-particles at time t_0. Based on the assumed concrete compositions, the total volume of cement paste is known. The difference between total cement paste volume and the uncarbonated volume of cement paste provides the amount of cement paste carbonated before time t_0. The CO_2 absorbed before time t_0 can be calculated as described in paragraph 2.5. This includes the carbonation in the concrete structure during its service life, the carbonation during and after demolition and the carbonation during crushing, sieving and piling before delivery to Empa and the handling in the laboratory at Empa. The results are presented in Table 5.

The percentage of CO_2 absorption respect to the original total emissions for RA-2 and RA-3 are close to the 10% calculated for the situation in Switzerland [10,12]. The absorbed CO_2 of RA-1 is considerably smaller. This can be explained by the differences in exposure conditions. The railway sleepers were exposed to unsheltered conditions, while it can be assumed that the majority of the concrete used to produce RA-2 and RA-3 originates from buildings. The major share of concrete in buildings is exposed to sheltered conditions where carbonation proceeds about twice as fast compared to unsheltered conditions [15]. Moreover, low quality concrete carbonates faster than high quality concrete [15] leading to a higher CO_2 absorption in RA-2 and RA-3 compared to RA-1.

4.4. Possible sources of error

During demolition, concrete sections in the size of about one meter long in their largest dimension are produced. After demolition, they are transported to a concrete plant. In the plant from which the RA for the project originates, demolished concrete is stored until its amount reaches 2000–4000 m^3 (4800–9600 tons). Then a mobile impact or cone

Table 5
CO_2 absorption of RA at the end of exposure in the plant: absolute value per mass of RA and relative values referred to the original emissions of concrete. Before and after t_0" refers to the time instant of the first measurement and hence roughly to the service life before demolition and storage as RA after crushing, respectively. Errors correspond to bootstrap 95% confidence intervals.

RA type	Before t_0			After t_0		
	CO_2 absorption [kg/t RA]	Relative to geogenic CO_2 [%]	Relative to total CO_2 [%]	CO_2 absorption [kg/t RA]	Relative to geogenic CO_2 [%]	Relative to total CO_2 [%]
RA-1, edge of pile	6.1 ± 3.5	8.0 ± 4.5	4.8 ± 2.7	10.0 ± 4.9	13.0 ± 6.3	7.9 ± 3.8
RA-1, interior of pile				9.9 ± 4.9	12.9 ± 6.3	7.8 ± 3.8
RA-2, edge of pile	13.4 ± 3.0	22.1 ± 4.9	13.3 ± 2.9	5.3 ± 4.1	8.8 ± 6.8	5.3 ± 4.1
RA-2, interior of pile				5.6 ± 4.1	9.2 ± 6.8	5.6 ± 4.1
RA-3, edge of pile	10.6 ± 3.0	17.4 ± 4.9	10.5 ± 2.9	12.5 ± 4.1	20.6 ± 6.8	12.4 ± 4.1
RA-3 interior of pile				9.7 ± 4.1	16.0 ± 6.8	9.6 ± 4.1

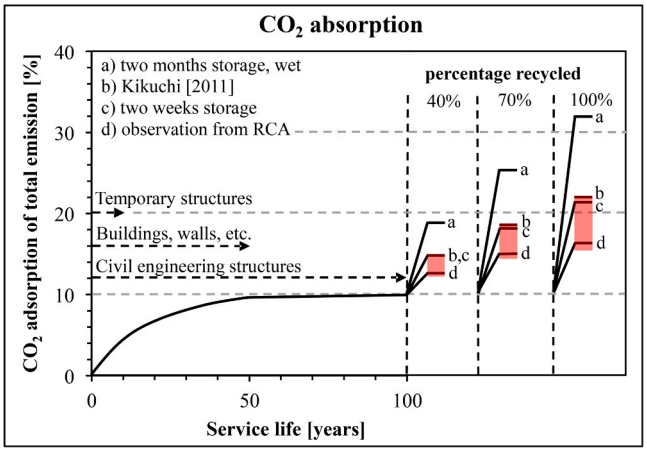

Fig. 13. Absorbed CO_2 relative to the total emission during the service life of concrete structures in Switzerland and during the recycling phase with rates of 40%, 70% and 100%. The range of values determined in this study are marked in red.
Figure adapted from [12].

crusher is installed in the plant to produce RA. Particles > 16 or 32 mm (depending on the plant) are crushed again. The producers of RA-1 and RA-2 separated a pile for the project. In plant-1 the pile encompassed about 2000 tons RA and in plant-2 about 150 tons. ~ 250 kg (RA-1) and ~ 75 kg (RA-2) were delivered to Empa at the start of the project. Two times ~ 100 kg (RA-1, edge and interior of the pile) and two times ~ 80 kg (RA-1) were delivered to Empa after the exposure in the plants. Although there is a certain homogenization in the entire production chain of RA, a certain sample variation between the first and the second delivery cannot be excluded. As only one delivery was used the above is not of concern for RA-3.

The pooled standard deviation of the carbonated RA determined with the method proposed here was 2.78 vol% (see paragraph 2.4). This leads to a relatively high error for lower volume-%. This error stems most likely from the intrinsic variability of the RA grains (see Figs. 8 and 9).

The calculation of CO_2 absorption is based on an assumed concrete mix design. A parameter with the most varying values reported and hence the one with the highest effect on the estimation is the amount of CaO converted to $CaCO_3$ in the carbonated cement paste (here assumed as 60%). The effect of this parameter can be however easily accounted for as the calculated CO_2 absorption is a linear function of the parameter (see Eq. 4). Hence, assuming the value of 75% instead of 60% would increase the estimated absorption 1.25 times. On the other hand, rather small relative differences are to be expected for the parameters of the concrete mix (cement content, w/c, air content) and hence they should have much lower effect on our estimations.

5. Summary

The amount of uncarbonated cement paste was determined on three different RA as a function of duration of exposure, exposure conditions and grain size class using a novel approach based on image analysis of the sections of RA particles treated with phenolphthalein. The changes in the amount of uncarbonated cement paste in the RA-particles during exposure made it possible to calculate CO_2 absorption assuming a certain concrete mix designs. The results improve the data base on experimentally determined natural CO_2 absorption during the recycling process. The following conclusions can be drawn in regard to the natural carbonation of RA:

- RA, in particular the fines, carbonate even when their moisture content is higher than the full water saturation (WA_{24}).
- Moist RA in sheltered exposure dries only slowly limiting the benefit of this storage type for increasing CO_2 absorption.
- Progress of carbonation slows down with time. About 80% of the cement paste carbonated until the end of storage (6 and 8 months, respectively) was already carbonated after 1.5 months.
- The highest amount of carbonated paste is formed in the sand (0–4 mm) representing 100% (RA-1), 53% (RA-2) and 61% (RA-3) on average of all grain size classes of the RA at the end of storage.
- The difference between the degree of carbonation at the edge of the pile (0–25 cm) is only marginally higher than in the interior of the pile (at a depth of 1.0–2.5 m).
- Sheltered RA carbonates only marginally faster than unsheltered RA during the chosen exposure durations.

The change in the volume of uncarbonated cement paste in the RA-particles allows to calculate CO_2 absorption of RA before and during exposure:

- The absorbed CO_2 during storage of the RA in the plants corresponds to a range of 9 – 21 ± 7% of the geogenic emission and 5 – 12 ± 4% of the total emission during clinker production (depending on the RA type and exposure, with errors corresponding to 95% confidence intervals).
- The absorbed CO_2 before crushing and storage corresponds to 8 – 22 ± 5% of the geogenic emission and 5 – 13 ± 3% of the total emission during clinker production. Although these numbers span a similar range as those corresponding to absorption after crushing and during storage as RA, they will strongly depend on the actual exposure conditions during service life for a particular type of RA.

6. Outlook

The types of concrete used and the demolition and recycling processes in different countries vary. Therefore, it is essential that the data base on natural CO_2 absorption is further improved by experimental data. Additionally, it may be of particular interest, how the degree of natural carbonation of the RA influences the potential to subsequently sequester CO_2 by accelerated carbonation.

CRediT authorship contribution statement

Andreas Leemann: Conceptualization; Formal analysis; Funding acquisition; Investigation; Methodology; Project administration; Resources; Validation; Visualization; Roles/Writing - original draft; Writing - review & editing. Beat Münch: Investigation; Methodology; Software; Validation; Visualization; Roles/Writing - original draft. Mateusz Wyrzykowski: Data curation; Formal analysis; Software; Validation; Visualization; Roles/Writing - original draft; Writing - review & editing.

Declaration of Competing Interest

The authors declare the following financial interests/personal relationships which may be considered as potential competing interests: Andreas Leemann reports financial support was provided by CemSuisse.

Data availability

Data will be made available on request.

Acknowledgement

The funding by cemsuisse is gratefully acknowledged. The authors thank Prof. Pietro Lura (Empa) for reviewing the manuscript.

References

[1] E. Elhacham, L. Ben-Uri, J. Grozovski, Y.M. Bar-On, R. Milo, Global human-made mass exceeds all living biomass, Nature 588 (7838) (2020) 442–444, https://doi.org/10.1038/s41586-020-3010-5.

[2] U.N. Environment, K.L. Scrivener, V.M. John, E.M. Gartner, Eco-efficient cements: Potential economically viable solutions for a low-CO_2 cement-based materials industry, Cem. Conc. Res 114 (2018) 2–26, https://doi.org/10.1016/j.cemconres.2018.03.015.

[3] WBCSD, Cement Sustainability Initiative, Getting the Numbers Right, Project Emissions Report 2014, ⟨http://www.gnr-project.org/⟩, (2016).

[4] M.J. Gibbs, P. Soyka, D. Conneely, Good practice guidance and uncertainty management in national greenhouse gas inventories, CO_2 Emiss. Cem. Prod. (2023). ⟨https://www.ipcc-nggip.iges.or.jp/public/gp/bgp/3_1_Cement_Production.pdf⟩.

[5] C. Le Quéré, R.M. Andrew, J.G. Canadell, S. Sitch, R.F. Keeling, Global carbon budget 2018, Earth Syst. Sci. Data 10 (2018) 2141–2194, https://doi.org/10.5194/essd-10-2141-2018.

[6] IEA, Technology Roadmap - Low-Carbon Transition in the Cement Industry IEA, Paris (2018) ⟨https://www.iea.org/reports/technology-roadmap-low-carbon-transition-in-the-cement-industry⟩.

[7] P. Friedlingstein, M. O'Sullivan, M.W. Jones, R.M. Andrew, J. Hauck, A. Olsen, G. P. Peters, W. Peters, J. Pongratz, S. Sitch, C. Le Quéré, Global carbon budget 2020, Earth Syst. Sci. Data 12 (4) (2020) 3269–3340.

[8] B. Lagerblad, Carbon dioxide uptake during concrete life cycle – state of the art. Swedish Cement and Concrete Research Institute CBI, Stockholm, 2005.

[9] C. Pade, M. Guimaraes, The CO_2 uptake of concrete in a 100 year perspective, Cem. Conc. Res. 37 (9) (2007) 1348–1356, https://doi.org/10.1016/j.cemconres.2007.06.009.

[10] P. Nygaard, A. Leemann, Kohlendioxidaufnahme von Stahlbeton durch Karbonatisierung, Cemsuisse Projekt 201106, Bern, 2012.

[11] C. Andrade, M. Sanjuán, Updating carbon storage capacity of spanish cement, Sustainability 10 (2018) 4806, https://doi.org/10.3390/su10124806.

[12] A. Leemann, CO2 absorption of concrete based on the boundary conditions of Switzerland, International Workshop, CO2 Storage in Concrete – CO2STO2019, Marne La Vallée, France, 2019.

[13] H.J. Wierig, Longtime studies on the carbonation of concrete under normal outdoor exposure, Proc. RILEM Seminar on the Durability of Concrete Structures under Normal Outdoor Exposure, 1984, pp. 239–249.

[14] V.G. Papadakis, M.N. Fardis, C.G. Vayenas, Effect of composition, environmental factors and cement-lime mortar coating on concrete carbonation, Mater. Struct. 25 (1992) 293–304, https://doi.org/10.1007/BF02472670.

[15] A. Leemann, F. Moro, Carbonation of concrete: the role of CO_2 concentration, relative humidity and CO_2 buffer capacity, Mater. Struct. 50 (1) (2017) 1–14, https://doi.org/10.1617/s11527-016-0917-2.

[16] Q.H. Vu, G. Pham, A. Chonier, E. Brouard, S. Rathnarajan, R. Pillai, R. Gettu, M. Santhanam, F. Aguayo, K.J. Folliard, M.D. Thomas, Impact of different climates on the resistance of concrete to natural carbonation, Constr. Build. Mater. 216 (2019) 450–467, https://doi.org/10.1016/j.conbuildmat.2019.04.263.

[17] P. Liu, Z. Yu, Y. Chen, Carbonation depth model and carbonated acceleration rate of concrete under different environment, Cem. Concr. Compos. 114 (2020), 103736, https://doi.org/10.1016/j.cemconcomp.2020.103736.

[18] K.O. Kjellsen, M. Guimaraes, A. Nilsson, The CO2 balance of concrete in a life cycle perspective, Danish Technological-DTI, 2005.

[19] T. Kikuchi, Y. Kuroda, Carbon dioxide uptake in demolished and crushed concrete, J. Adv. Concr. Tech. 9 (1) (2011) 115–124, https://doi.org/10.3151/jact.9.115.

[20] M. Thiery, P. Dangla, P. Belin, G. Habert, N. Roussel, Carbonation kinetics of a bed of recycled concrete aggregates: a laboratory study on model materials, Cem. Concr. Res. 46 (2013) 50–65, https://doi.org/10.1016/j.cemconres.2013.01.005.

[21] R. Andersson, K. Fridh, H. Stripple, M. Häglund, Calculating CO_2 uptake for existing concrete structures during and after service life, Environ. Sci. Technol. 47 (20) (2013) 11625–11633, https://doi.org/10.1021/es401775w.

[22] K.H. Yang, E.A. Seo, S.H. Tae, Carbonation and CO_2 uptake of concrete, Environ. Impact Asses. 46 (2014) 43–52, https://doi.org/10.1016/j.eiar.2014.01.004.

[23] C. Shi, Y. Li, J. Zhang, W. Li, L. Chong, Z. Xie, Performance enhancement of recycled concrete aggregate - a review, J. Clean. Prod. 112 (2016) 466–472, https://doi.org/10.1016/j.jclepro.2015.08.057.

[24] V.W. Tam, A. Butera, K.N. Le, W. Li, Utilising CO_2 technologies for recycled aggregate concrete: A critical review, Constr. Build. Mater. 250 (2020), 118903, https://doi.org/10.1016/j.conbuildmat.2020.118903.

[25] B. Lei, W. Li, Z. Luo, V.W. Tam, W. Dong, K. Wang, Performance enhancement of permeable asphalt mixtures with recycled aggregate for concrete pavement application, Front. Mater. 7 (2020) 253, https://doi.org/10.3389/fmats.2020.00253.

[26] Y. Pu, L. Li, Q. Wang, X. Shi, C. Luan, G. Zhang, L. Fu, A.E.F. Abomohra, Accelerated carbonation technology for enhanced treatment of recycled concrete aggregates: A state-of-the-art review, Constr. Build. Mater. 282 (2021), 122671, https://doi.org/10.1016/j.conbuildmat.2021.122671.

[27] V.W. Tam, A. Butera, K.N. Le, W. Li, CO_2 concrete and its practical value utilising living lab methodologies, Clean. Eng. Technol. 3 (2021), 100131, https://doi.org/10.1016/j.cemconcomp.2022.104629.

[28] Z. Ma, J. Shen, C. Wang, H. Wu, Characterization of sustainable mortar containing high-quality recycled manufactured sand crushed from recycled coarse aggregate, Cem. Concr. Compos. 132 (2022), 104629, https://doi.org/10.1016/j.cemconcomp.2022.10462.

[29] H. Wu, R. Hu, D. Yang, Z. Ma, Micro-macro characterizations of mortar containing construction waste fines as replacement of cement and sand: A comparative study, Constr. Build. Mater. 383 (2023), 131328, https://doi.org/10.1016/j.conbuildmat.2023.131328.

[30] EN 933–1:2012, Tests for geometrical properties of aggregates - Part 1: Determination of particle size distribution - Sieving method.

[31] EN 1097–6:2014, Tests for mechanical and physical properties of aggregates - Part 6: Determination of particle density and water absorption.

[32] M.K. Agoston, Computer Graphics and Geometric Modeling: Implementation and Algorithms, Springer,, London, 2005, pp. 300–306.

[33] M.R. Chernick, Bootstrap Methods: A Guide For Practitioners And Researchers, John Wiley & Sons,, 2011.

[34] FprEN 16757:2021, CEN/TC 229 Sustainability of construction works - Environmental product declarations Product Category Rules for concrete and concrete elements.

[35] EN 206:2013+A2:2021, Concrete - Specification, performance, production and conformity (available in German and French).

[36] M. Castellote, C. Andrade, X. Turrillas, J. Campo, G.J. Cuello, Accelerated carbonation of cement pastes in situ monitored by neutron diffraction, Cem. Conc. Res 38 (12) (2008) 1365–1373, https://doi.org/10.1016/j.cemconres.2008.07.002.

[37] A. Leemann, H. Pahlke, R. Loser, F. Winnefeld, Carbonation resistance of mortar produced with alternative cements, Mater. Struct. 51 (5) (2018) 1–12, https://doi.org/10.1016/j.cemconres.2013.01.005.

[38] C.F. Chang, J.W. Chen, The experimental investigation of concrete carbonation depth, Cem. Concr. Res. 36 (9) (2006) 1760–1767, https://doi.org/10.1016/j.cemconres.2004.07.025.

[39] Z. Shi, B. Lothenbach, M.R. Geiker, J. Kaufmann, A. Leemann, S. Ferreiro, J. Skibsted, Experimental studies and thermodynamic modeling of the carbonation of Portland cement, metakaolin and limestone mortars, Cem. Concr. Res. 88 (2016) 60–72, https://doi.org/10.1016/j.cemconres.2016.06.006.

[40] E. Thomson, Quantitative microscopic analysis, J. Geol. 38 (3) (1930) 193–222, https://doi.org/10.1086/623710.

[41] S. Steiner, B. Lothenbach, T. Proske, A. Borgschulte, F. Winnefeld, Effect of relative humidity on the carbonation rate of portlandite, calcium silicate hydrates and ettringite, Cem. Concr. Res. 135 (2020), 106116, https://doi.org/10.1016/j.cemconres.2020.106116.

[42] R. Kündig et al. Die mineralischen Rohstoffe der Schweiz, Zürich, Schweizerische Geotechnische Kommission, 1997.